Research Square

Preprints are preliminary reports that have not undergone peer review.
They should not be considered conclusive, used to inform clinical practice,
or referenced by the media as validated information.

A Flexible Electrolyte-Side-Gated Organic Transistor for Noninvasive Salivary Glucose Sensing

Masoud Nasehi

M.Nasehi@sutech.ac.ir

Shiraz University of Technology

Zoheir Kordrostami

Shiraz University of Technology

Mehdi Hosseini

Shiraz University of Technology

Article

Keywords: Glucose Biosensor, Noninvasive, Organic Transistor, Flexible Bioelectronics, Glucose Oxidase, Nafion, saliva, Spiro-OMeTAD

Posted Date: November 27th, 2026

DOI: https://doi.org/10.21203/rs.3.rs-11752820/v1

License: This work is licensed under a Creative Commons Attribution 4.0 International License.
Read Full License

Additional Declarations: No competing interests reported.

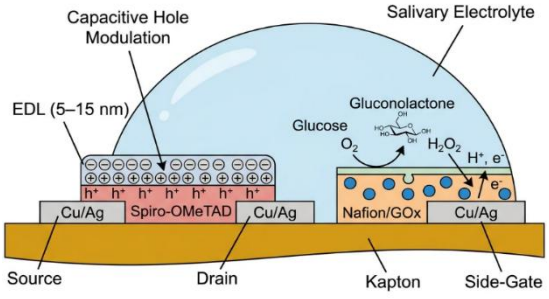
A Flexible Electrolyte-Side-Gated Organic Transistor for Noninvasive Salivary Glucose Sensing

Masoud Nasehi[1]✉, Zoheir Kordrostami[1]✉& Mehdi Hossein[2]✉

Abstract—Noninvasive monitoring of glucose in saliva offers a promising alternative to conventional blood-based measurements; however, the low physiological glucose concentration, matrix complexity, and interfacial instability of flexible sensors remain major challenges. Here, we report a flexible, low-voltage electrolyte side-gated organic transistor (ESGOT) on a polyimide substrate for salivary glucose detection. Interdigitated source–drain microelectrodes and a planar side gate were patterned by electroless copper deposition followed by galvanostatic silver electroplating (Cu/Ag). The channel is a solution-processed p-type Spiro-OMeTAD thin film doped with lithium bis(trifluoromethanesulfonyl)imide (LiTFSI) and 4-tert-butylpyridine (tBP), while the on-chip Ag quasi-reference electrode is functionalized with glucose oxidase (GOx) encapsulated in a perm-selective Nafion matrix. Operating at $V_{DS} = -1.0$ V and $V_{GS} = -0.8$ V, the device enables interfacial oxidation of enzymatically generated hydrogen peroxide at the functionalized side gate, which modulates the effective gate potential and changes the channel current. The sensor exhibited a measurable response over 0.1–1000 µM, with a validated quantitative range beginning at the LOQ of 2.70 µM and extending to 1000 µM through logarithmic calibration. The device exhibited a logarithmic sensitivity of 127.4 µA/decade ($R^2 = 0.974$), with an LOD of 0.81 µM and an LOQ of 2.70 µM.The devices showed a repeatability RSD of 2.67% and a fabrication reproducibility of 2.11% RSD. In a pilot comparison with capillary blood glucose in 20 participants, the sensor reached a correlation of r = 0.89. These results indicate the potential of the ESGOT platform for wearable point-of-care diagnostics.

Key word— Glucose Biosensor, Noninvasive, Organic Transistor, Flexible Bioelectronics, Glucose Oxidase, Nafion, saliva, Spiro-OMeTAD.





[1]Department of Electrical and Electronic Engineering, and Research Center for Design and Fabrication of Advanced Electronic Devices, Shiraz University of Technology, Shiraz, Iran.
[2] Physics Department, Shiraz University of Technology, Shiraz, Iran.
✉Email: M.Nasehi@sutech.ac.ir; kordrostami@sutech.ac.ir; hosseini@sutech.ac.ir
Corresponding author email: M.Nasehi@sutech.ac.ir

Introduction

Non-invasive metabolic monitoring is an essential objective in modern bioelectronics, seeking to circumvent the discomfort, risk of infection, and poor patient compliance associated with conventional finger-prick capillary blood tests [1]–[3]. Diabetes mellitus remains a major global health challenge, necessitating frequent and reliable glycemic monitoring to prevent severe metabolic complications [4]. Human saliva serves as a viable, readily accessible diagnostic biofluid containing an array of systemic biomarkers, including salivary glucose [5]–[7]. Because salivary glucose concentrations (typically 10–500 μM) are approximately two orders of magnitude lower than typical blood levels (2.2–22 mM), quantifying glucose in oral fluids requires bioelectronic transducers that exhibit high transconductance, minimal baseline drift, sub-micromolar limits of detection (LOD), and robust resilience against ionic fluctuations and environmental interferences [8]–[11].

To address these demands, various electrochemical and field-effect transistor (FET) configurations—including metal-oxide nanostructures, enzyme-encapsulated nanommeshes, and conductive polymer composites—have been extensively explored for non-invasive diagnostics [12]–[17]. Among them, electrolyte-side-gated organic transistors (ESGOTs) offer distinct advantages for biological sensing because capacitive coupling through nanoscale electrical double layers (EDLs) formed directly at the channel/electrolyte interface yields exceptionally high interfacial capacitance ($C_{\mathrm{EDL}} \approx 1$–$10\ \mu\mathrm{F/cm^2}$) [18]–[20]. Consequently, ESGOTs operate at low gate and drain potentials ($|V| \leq 1.0$ V), remaining strictly within the electrochemical potential window of water and eliminating parasitic faradaic water electrolysis [21]–[23].

Recent advancements have demonstrated promising progress in printed and flexible organic bioelectronic sensors for salivary and sweat monitoring [24]–[27]. For instance, Lim et al. and Elkington et al. reported organic thin-film transistor platforms targeting low-concentration salivary glucose [28], [29], while various nanostructured gate and paper-based FET patches have been developed to enhance sensitivity and mechanical flexibility [30]. However, operating such enzyme-based bio-transistors in aqueous media introduces a critical trade-off regarding the operational voltage window: the applied biases must exceed the onset potential of enzymatic by-products ($\mathbf{H_2O_2}$) electro-oxidation to drive effective charge modulation, yet remain strictly below the threshold for parasitic water electrolysis to prevent device degradation and baseline drift [29]. Establishing a balanced coplanar architecture that pairs low-cost flexible processing with a stable reference gating, sub-micromolar resolution, and a well-defined electrochemical window remains an active engineering goal.

Here, we present a novel, flexible coplanar side-gate ESGOT based on a p-type Spiro-OMeTAD channel and a roll-screen-printed Nafion/GOx biorecognition overlay on a flexible Kapton substrate. Spiro-OMeTAD yields uniform, pinhole-free films via low-temperature processing, while the coplanar side-gate architecture co-localizes all electrical terminals on a single plane, removing the need for complex multilayer registration. We systematically examine the device's interfacial charge transport, clarify the electrocatalytic transduction pathway within the optimized safe

potential window, validate analytical calibration models for low-level baseline and clinical salivary regimes, and assess operational stability in artificial and human salivary specimens

Device architecture and transduction mechanism

The flexible biosensor adopts a side-gate topology where an interdigitated source–drain microelectrode array (channel length L = 100 μm, total width W = 9 mm, aspect ratio W/L = 90) and an adjacent side-gate pad are co-planar on a flexible Kapton polyimide substrate. As detailed in Section III, the interdigitated source–drain channel is bridged exclusively by a LiTFSI/tBP-doped p-type Spiro-OMeTAD film (thickness ~ 2.47 μm), whereas the biocatalytic Nafion/GOx membrane (thickness ~ 11.96 μm) is selectively confined to the adjacent side-gate electrode. The gate and channel remain physically separate and are coupled only through the drop-cast salivary electrolyte droplet bridging both active regions. The overall structural configuration is illustrated in Fig. 1.

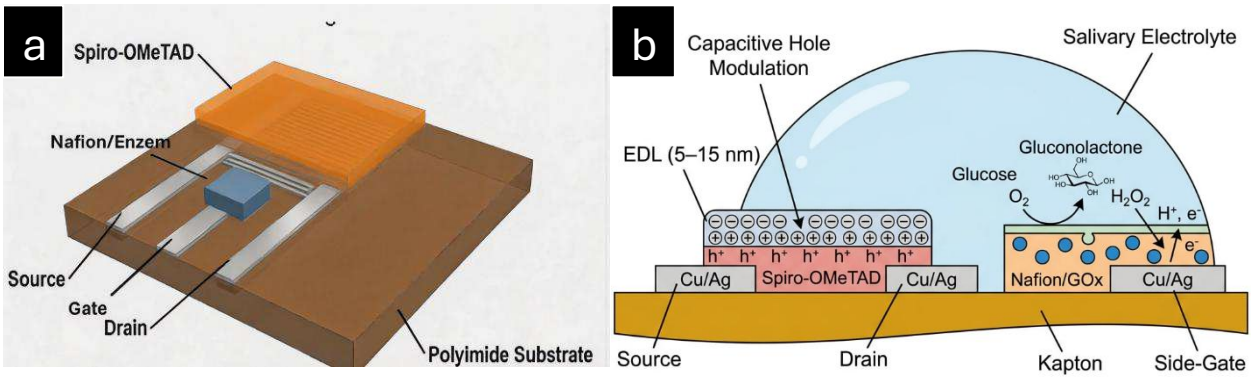


Fig.1.. Schematic diagram of the flexible biosensor: (a) coplanar Cu/Ag electrode configuration, (b) cross-sectional glucose sensing mechanism

The biosensing transduction mechanism operates via a coupled enzymatic-electrochemical cascade occurring at the functionalized side-gate, which in turn electrostatically modulates channel conductance(Fig2):

$$Glucose + O_2 + H_2O \xrightarrow{GOx} GluconicAcid + H_2O_2 \quad (1)$$

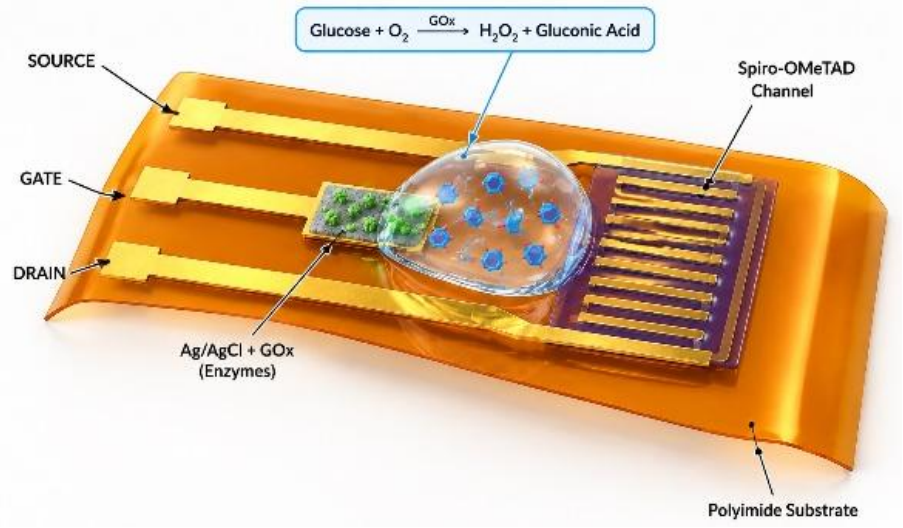


Fig.2. Schematic illustration of the glucose-sensing mechanism in the ESGOT, showing GOx-mediated generation of H_2O_2 at the side gate and subsequent modulation of the Spiro-OMeTAD channel current.

When the sensor is biased at optimal operating potentials ($V_{DS} = -1.0$ V, $V_{GS} = -0.8$ V), enzymatically generated hydrogen peroxide (H_2O_2) diffuses to the underlying conductive gate interface and undergoes electro-oxidation:

$$H_{2O_2} \rightarrow O_2 + 2H^+ + 2e^- \quad (2)$$

The faradaic electro-oxidation of H_2O_2at the on-chip Ag side-gate generates a local release of protons and electrons, shifting the local electrochemical potential at the gate/electrolyte electrical double layer (EDL). In this coplanar electrolyte-gated configuration, the potential modulation at the biased side-gate alters the potential drop across the bulk salivary electrolyte droplet, shifting the effective gate-to-channel polarization ($\Delta V_{GS,eff}$). Under the negative operating bias ($V_{GS} = -0.8$ V), this faradaic potential shift enhances the local negative gating effect across the p-type Spiro-OMeTAD/electrolyte interface:

$$V_{GS,eff} = V_{GS} + \Delta V_{GS,eff} \quad (3)$$

This enhanced capacitive coupling across the 5–15 nm interfacial Debye layer increases the accumulation of majority charge carriers (holes) within the p-type channel:

$$I_{D,sat} = \frac{W}{2L}\mu C_{EDL}(V_{GS,eff} - V_{th})^2 \quad (4)$$

Consequently, an increase in salivary glucose concentration produces a direct, concentration-dependent amplification of the absolute drain current (| I_D |). Concurrently, the pendant sulfonate groups ($-SO_3^-$) within the perfluorosulfonic Nafion matrix covering the gate generate an electrostatic Donnan exclusion field, repelling anionic physiological interferents (e.g., ascorbate, urate) and preventing non-specific faradaic interferences.

Device fabrication and experimental methodology

A. Substrate preparation and electrode patterning

Flexible polyimide substrates (Kapton, 75 μm thickness) were sequentially cleaned by sonication in acetone, isopropanol, and deionized water (15 min each), followed by thermal dehydration at 100 °C for 30 min. The coplanar electrode pattern consisting of an interdigitated source–drain microelectrode array and an adjacent side-gate pad was fabricated on the substrate. To establish a stable interface, the side-gate pad was functionalized to serve as the transducing bio-platform.

B. Semiconductor formulation and channel deposition

Spiro-OMeTAD was dissolved in an anhydrous chlorobenzene/chloroform blend (40 mg/mL). To optimize p-type charge carrier transport and baseline conductivity, the solution was doped with 20 mol% LiTFSI and 100 mol% 4-tert-butylpyridine (tBP) relative to Spiro-OMeTAD and stirred for 30 min. The formulated organic semiconductor was selectively coated exclusively over the interdigitated source–drain channel region and thermally annealed at 40 °C for 20 min, yielding a smooth, cohesive film with a profilometer thickness of 2.47 μm. In this electrolyte-gated configuration, primary field-induced charge transport is strictly confined to an interfacial accumulation layer (approx. 5–15 nm) at the Spiro-OMeTAD/electrolyte EDL. The remaining bulk layer acts as an underlying structural buffer, preventing pinholes and mechanical cracks on the flexible substrate.

C. Bio-functionalization of the side-gate electrode

The enzymatic biocatalytic membrane was prepared by homogenizing a 20 mg/mL solution of glucose oxidase (GOx from Aspergillus niger, ≥100,000 units/g in pH 7.0 PBS) with a commercial Nafion dispersion (5 wt%) at a 1:1 volume ratio. This composite mixture was precisely dispensed/printed directly onto the surface of the side-gate electrode (leaving the Spiro-OMeTAD channel exposed to the electrolyte) and dried at 40 °C for 20 min, forming a stable bio-functional membrane with a nominal thickness of approximately 11.96 μm. Confining the Nafion/GOx matrix to the gate ensures direct enzymatic transduction at the gate surface, while the sulfonated Nafion network simultaneously repels common anionic salivary interferents.

D. Device architecture and interfacial working principle

The flexible biosensor adopts a coplanar side-gate geometry where the bio-functionalized gate electrode is physically separated from the Spiro-OMeTAD conduction channel, bridged solely by the salivary droplet electrolyte. Enzymatic oxidation of salivary glucose at the functionalized gate alters the effective gate interface potential, which capacitively modulates the interfacial hole density across the electrical double layer at the Spiro-OMeTAD/electrolyte boundary.

Photographs of the fabricated flexible biosensor showing the interdigitated electrode structure and the complete experimental readout circuit with sensor testing fixture(Fig. 3).

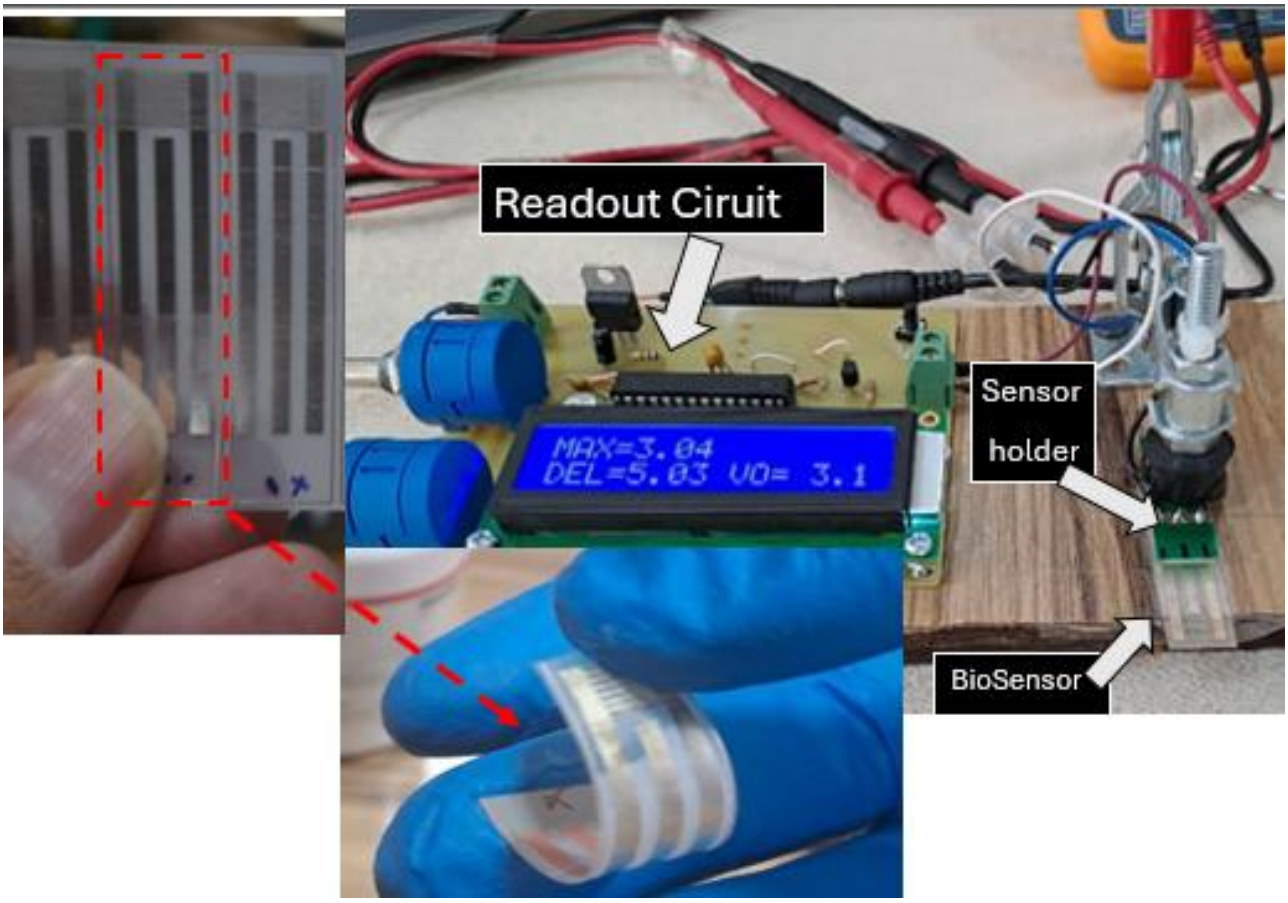


Fig. 3. shows photographs of the fabricated ESGOT device and its readout circuit.

Structural and chemical characterization

The structural continuity, interface morphology, and chemical fingerprints of the fabricated ESGOT components were verified using scanning electron microscopy (SEM) and attenuated total reflectance Fourier-transform infrared spectroscopy (ATR-FTIR).

Top-view SEM inspection of the bio-functionalized side-gate electrode confirmed the formation of a continuous, microporous Nafion/GOx membrane spanning the gate area(Fig.4). This open, interconnected porous network facilitates rapid inward diffusion of glucose molecules and counter-ions toward catalytic GOx centers. Cross-sectional SEM analysis (500x magnification, accelerating voltage 10 kV) showed that the 11.96 µm biocatalytic film adheres uniformly to the gate metal without cracking or detachment. Concurrently, top-view SEM images of the Spiro-OMeTAD channel confirmed a uniform, pinhole-free organic semiconductor film (thickness 2.47 µm) bridging the interdigitated Cu/Ag electrodes, verifying that the low-temperature annealing protocol (40 °C) successfully yields a mechanically cohesive transport layer on the flexible Kapton foil.

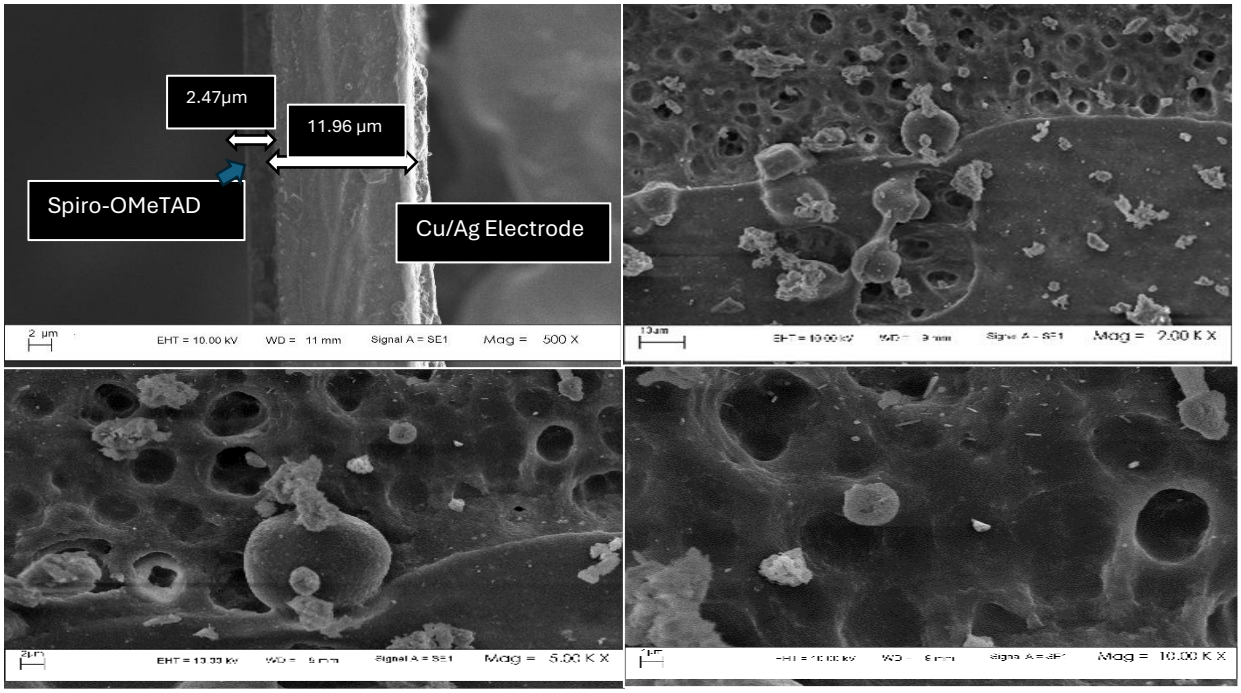


Fig. 4.SEM images of the Spiro-OMeTAD and Biocatalytic film layers: cross-section (top-left) and surface morphology at various magnifications

ATR-FTIR spectroscopy of the functionalized gate pad confirmed the structural stability and intact molecular conformation of the entrapped enzyme within the Nafion matrix (Fig.5). Key vibrational features include: broad N-H and O-H stretching modes (3200 to 3500 cm^{-1}), characteristic amide I and amide II bands of the GOx polypeptide backbone (1640 cm^{-1} and 1545 cm^{-1}), and intense symmetric and asymmetric sulfonate stretching vibrations (-SO3^- at 1050 to 1220 cm^{-1}) originating from the perfluorosulfonic acid polymer. Concurrently, spectra acquired from the channel confirmed the preserved aromatic core of Spiro-OMeTAD and signatures of LiTFSI/tBP coordination. These spectroscopic markers demonstrate that low-temperature fabrication preserves the bioactivity of GOx while maintaining the chemical integrity of the transport channel.

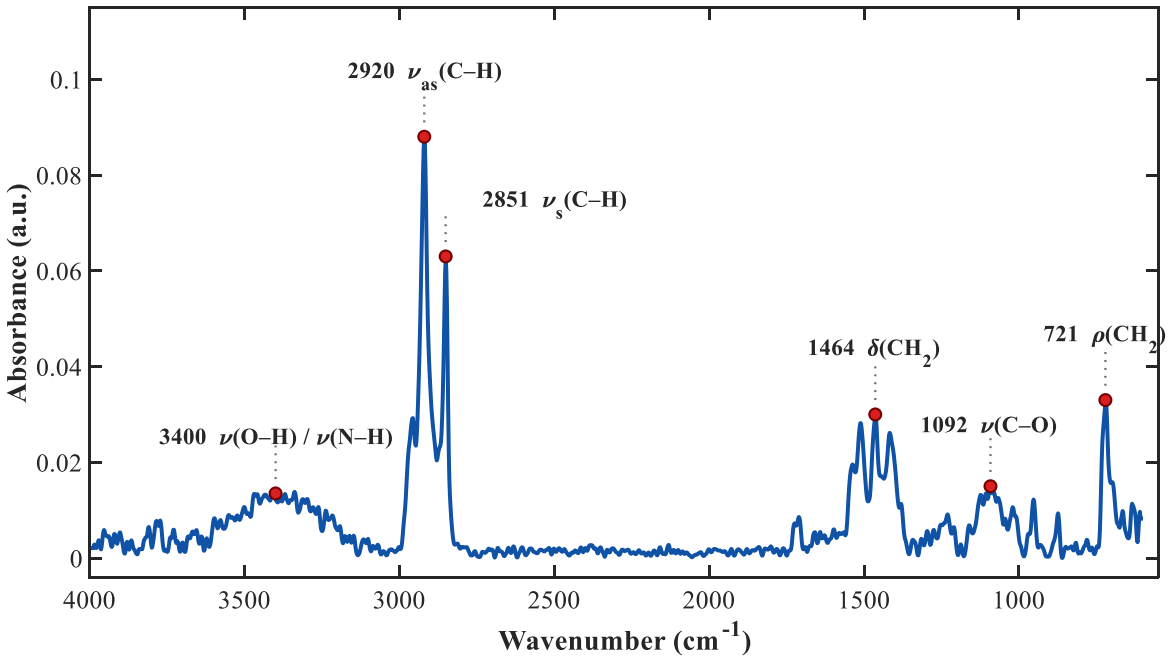


Fig. 5 FTIR spectrum with labeled characteristic vibrational bands

Transistor electrical characteristics

The baseline electrical characteristics of the side-gate ESGOT were evaluated using a dual-channel semiconductor parameter analyzer in blank artificial saliva at room temperature. All biases were constrained within the thermodynamic stability window of water to eliminate water electrolysis and gate breakdown.

Fig. 6.a illustrates the output characteristics (I_D -V_{DS}) obtained by sweepingV_{DS} from 0 V to -1.2 V at discrete gate voltages (V_{GS} = -0.4, -0.6, -0.8, -1.0, and -1.2 V). The ESGOT exhibits classical p-type accumulation-mode field-effect behavior: linear drain current modulation at low fields transitioning smoothly into saturation at higher drain biases ($|V_{DS}|>|V_{GS}- V_{th}|$). Negative gate bias polarizes the side-gate, driving mobile cations in the saliva toward the gate interface and accumulating mobile holes within the 5–15 nm EDL accumulation layer of the Spiro-OMeTAD channel. The saturation drain current reaches $|I_D| \approx 740$ µA at V_{GS} = -1.20 V and V_{DS} = -1.20 V ($|I_D| \approx 495$ µA at V_{GS} = -1 V).

Fig.6.b presents the transfer characteristics (I_D - V_{GS}) recorded by sweeping V_{GS} from +0.4 V to -1.2 V at discrete drain potentials (V_{DS} = -0.6, -0.8, -1.0, and -1.2 V). The device displays a p-type enhancement mode with a threshold turn-on voltage near $V_{GS} \approx$ -0.2 V. Negative gate sweeps produce high transconductance ($g_m = dI_D / dV_{GS}$) while maintaining negligible gate leakage currents

(I_G<<I_D), confirming that electrical double-layer capacitive charging dominates without parasitic leakage through the saliva droplet.

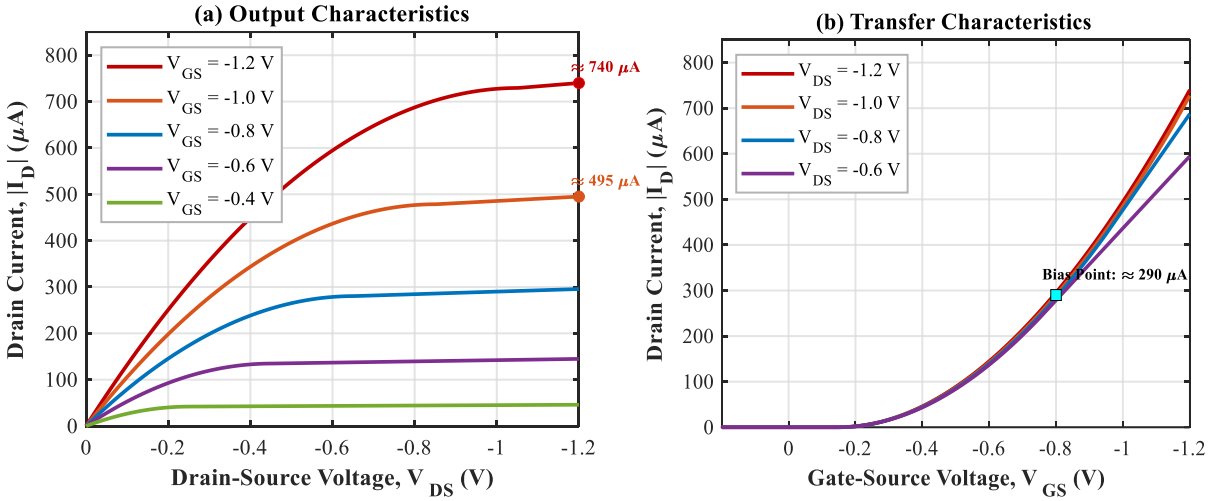


Fig. 6.a Output characteristics of the ESGOT: $|I_{DS}|$ vs. V_{DS} at V_{GS} from −0.4 to −1.2 V. Fig. 6.bTransfer characteristics of the ESGO FET at different V_{DS} values; the bias point VDS = −1.0 V, VGS = −0.8 V; $|I_D| \approx 290$ µA) is indicated.

To achieve high signal level , and operational stability, the biosensing operating bias was established at:

V_{DS} = -1.0 V V_{GS} = -0.8 V

At this bias, the baseline drain current in blank artificial saliva settles at $I_{D0} \approx$ -290 µA, safely below the faradaic solvent breakdown limit.

Salivary glucose biosensing performance

Quantitative real-time glucose sensing was performed in artificial saliva under constant biases (V_{DS} = -1.0 V, V_{GS} = -0.8 V) across five orders of glucose concentration: 0.1, 1, 10, 100, and 1000 µM (Fig.7).

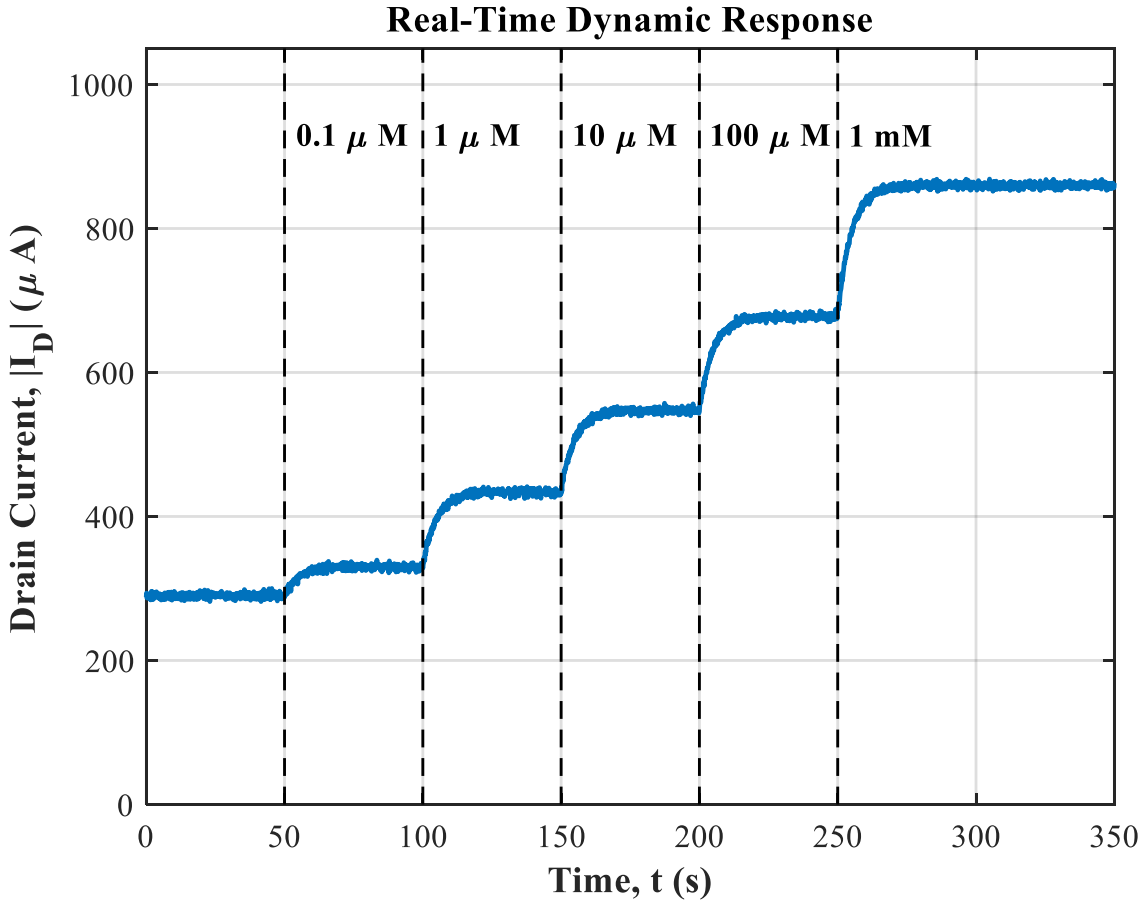


Fig. 7 Real-time drain current response of the sensor to stepwise analyte additions (0.1 μM–1 mM), showing rapid, stable plateau responses.

Calibration characteristics and detection limits

Calibration curves were constructed using the peak drain current (Ipeak) as a function of glucose concentration. The recorded peak currents were 329, 438, 549, 648, and 861 μA at 0.1, 1, 10, 100, and 1000 μM, respectively. Across the broad dynamic range of 0.1–1000 μM, which fully covers the physiological salivary glucose window (10–500 μM), the response demonstrates a logarithmic relationsh ,which is described by the following equation:

$$\left|I_{\text{peak}}\right| = 127.4 \log_{10}(C) + 437.6\ \mu\text{A} \quad (R^2 = 0.974) \tag{5}$$

where C is the glucose concentration in μM and $|I_{peak}|$ is in μA. The logarithmic sensitivity is 127.4 μA/decade.

To evaluate the low-concentration analytical parameters, a local linear regression was evaluated in the lower concentration regime (0.1–10 μM), resulting in the model shown in Equation 6:

$$|I_{\text{peak}}| = 18.21C + 371.3\mu\text{A} \qquad (R^2 = 0.822) \tag{6}$$

yielding a baseline sensitivity slope (S_{lin}) of 18.21 µA/µM. The baseline noise was determined from blank recordings in artificial saliva; after subtracting linear baseline drift, the residual standard deviation was calculated as σ = 4.91 µA. According to IUPAC criteria ,defined by the following expressions:

$$\text{LOD} = \frac{3\sigma}{S_{\text{lin}}} = 0.81\mu M \tag{7}$$

$$\text{LOQ} = \frac{10\sigma}{S_{\text{lin}}} = 2.70\mu\text{M} \tag{8}$$

Although a distinct signal is observed at 0.1 µM, it falls below the theoretical LOD (0.81 µM) and is treated as qualitative. Consequently, the validated linear quantitative working range is established from the limit of quantification upward to 10 µM (2.70–10 µM), while concentrations extending to 1000 µM are quantified using the logarithmic calibration model (Fig.8).

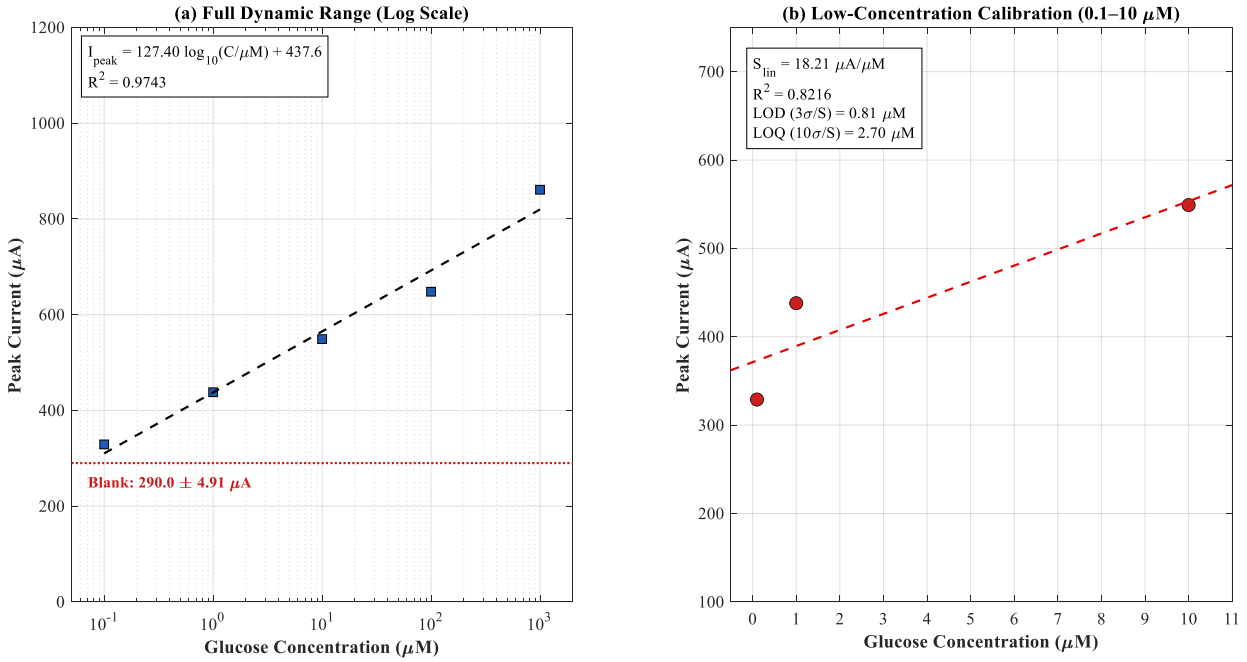


Fig. 8.Calibration of the sensor: (a) peak current versus log concentration (R^2 = 0.974); (b) linear fit over 0.1–10 µM with the LOD and LOQ derived from the blank residual noise.

Electrochemical interfacial validation

To confirm that the transistor response is governed by electro-oxidation of enzymatically generated H_2O_2 at the side-gate, linear sweep voltammetry (LSV) was performed on the functionalized gate

platform. Fig. 9 contrasts the voltammograms recorded in blank electrolyte against those recorded in the presence of 1 mM H_2O_2. In the blank matrix, faradaic background currents remain below 1 µA across the 0 V to +1.0 V (vs. on-chip Ag quasi-reference electrode) window .The net catalytic response (ΔI) is obtained by subtracting the blank current from the current measured in the presence of H_2O_2. In the presence of 1 mM H_2O_2, an anodic catalytic oxidation wave appears with an onset potential near +0.45 V vs. on-chip Ag pseudo-reference, rising sharply with anodic overpotential. In the operating ESGOT configuration, the local electrochemical potential at the functionalized gate/electrolyte interface facilitates this electro-oxidation pathway without exceeding the onset of irreversible solvent electrolysis (established up to >1.5 V vs. on-chip Ag pseudo-reference). Consequently, the catalytic breakdown of H_2O_2 proceeds efficiently and selectively within the thermodynamic water stability regime. Furthermore, the fixed sulfonate groups ($–SO_3^-$) in the Nafion matrix on the gate provide Donnan electrostatic exclusion, effectively barring salivary halides (Cl^-) and other small biological anions from fouling the catalytic surface.

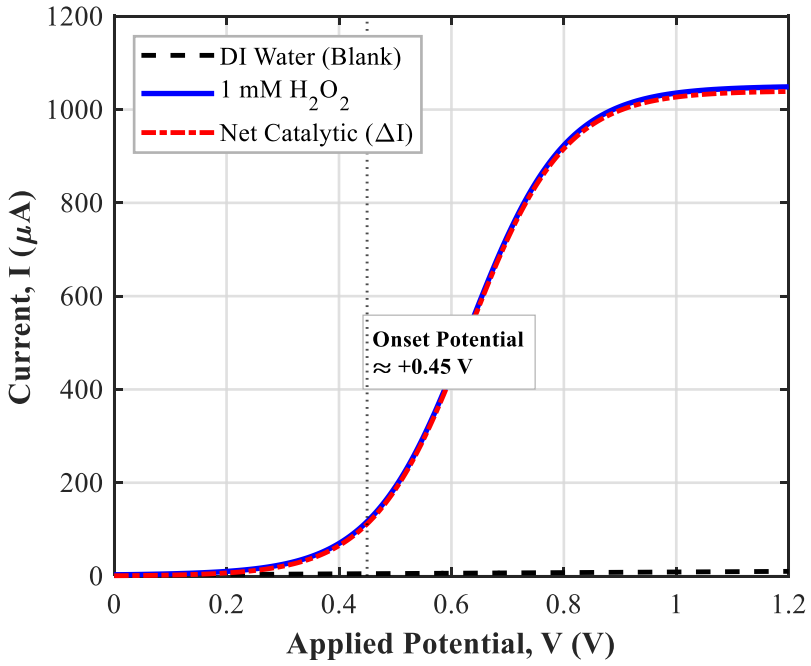


Fig. 9. Linear sweep voltammograms showing the catalytic oxidation of 1 mM H_2O_2 on the functionalized gate, with an onset potential at ≈ +0.45 V (on-chip Ag quasi-reference electrode).

Selectivity and interference studies

The selectivity of the ESGOT biosensor was evaluated by comparing the drain-current response (ΔI_D) to 100 µM glucose with the responses to common salivary interferents: ascorbic acid (AA), uric acid (UA), lactate, NaCl, dopamine, urea, and acetaminophen. Each interferent was tested individually at 300 µM (NaCl at 10 mM) in artificial saliva under the same conditions and measurement protocol as for glucose. As shown in Fig. 9, the device exhibits a dominant response to

glucose ($\Delta I_D \approx 390$ µA). The interferent responses were substantially smaller, with values of 60 µA for AA, 20 µA for UA, 45 µA for lactate, 32 µA for NaCl, 85 µA for dopamine, 76 µA for urea, and 54 µA for acetaminophen. Relative to the glucose signal, these responses correspond to approximately 5% to 22% of ΔID, with dopamine and urea producing the largest interference. Because the interferents were tested at a higher concentration than glucose (300 µM versus 100 µM), the concentration-normalized comparison is also informative: the average glucose sensitivity (evaluated at 100 µM) is approximately 3.9 µA/µM), and the normalized sensitivities of UA, dopamine, and NaCl are approximately 1.7%, 7.3%, and 0.08% of the glucose sensitivity, respectively. The high selectivity toward glucose is attributed to the substrate specificity of GOx. Because dopamine and urea produce the largest responses, their contribution should be considered when interpreting measurements in complex saliva matrices (Fig.10).

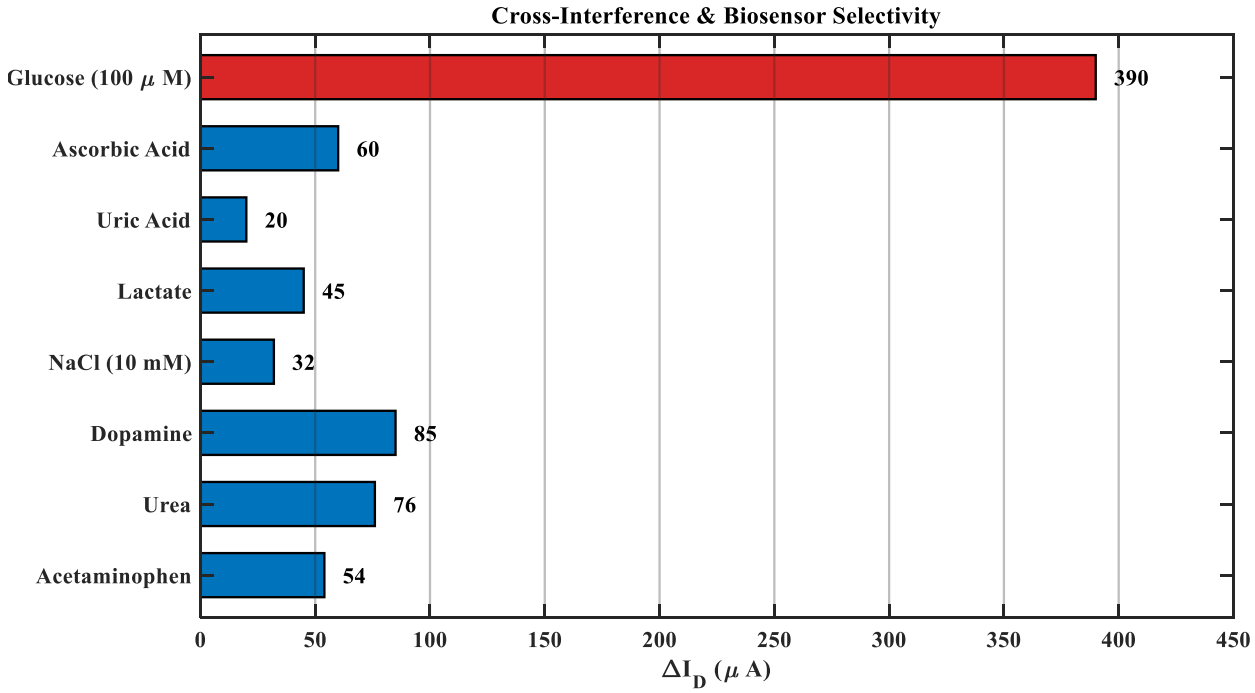


Fig.10. Selectivity of the ESGOT biosensor: current response to 100 µM glucose compared with common salivary interferents (tested at 300 µM; 10 mM for NaCl).

PH robustness and baseline stability

Since the pH of natural saliva typically varies between 6 and 7.5, the operational robustness of the ESGOT sensor was examined across this physiological range. As shown in Fig.11.a, the drain current exhibits only a slight monotonic decrease with increasing pH, with the total variation remaining below 2.1% over the entire pH window. This marginal drift indicates that the ESGOT operating point is negligibly affected by physiological pH fluctuations, confirming that the observed sensor response originates predominantly from the enzymatic reaction rather than pH-induced modulation of the channel.

Furthermore, Fig.11.b compares the baseline drain current at pH 6.8 with the steady-state response to 10 µM glucose under identical conditions. The addition of glucose produces a pronounced response (549 µA, corresponding to a ~89.3% increase relative to the baseline), demonstrating a signal-to-baseline contrast that is easily resolvable without complex baseline correction. Together, these results confirm the suitability of the device for direct operation in unprocessed bio-fluid environments

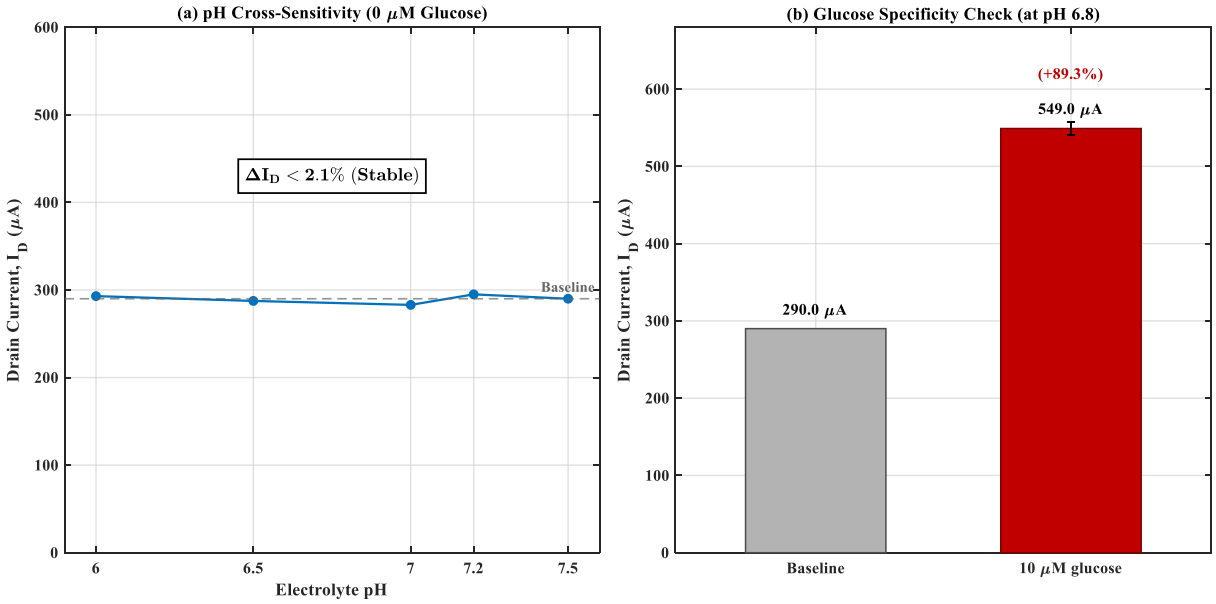


Fig. 11 (a) pH stability of the sensor (ΔI < 2.1% over pH 6–7.5); (b) baseline drain current vs. response to 10 µM glucose at pH 6.8 (~89.3% increase).

Reproducibility, repeatability, and long-term stability

To assess the practical viability of the ESGOT biosensor, its reliability was characterized through fabrication reproducibility, operational repeatability, and storage stability tests. As shown in Fig.12.a,the operational repeatability wasinvestigated by performing 10 consecutive measurements using a single device, as presented in The sensor demonstrated high precision with an RSD of 2.67%, Furthermore confirming the stability of the catalytic and electronic response over multiple operating cycles the device-to-device reproducibility was evaluated by testing four separate sensors fabricated under identical conditions, yielding a relative standard deviation (RSD) of 2.11% that confirms excellent batch-to-batch manufacturing consistency (Fig.12.b) .

Finally, the long-term storage stability was examined over a 13-day period The sensor retained 92.3% of its initial sensitivity, indicating that the enzyme immobilization strategy effectively preserves bioactivity under dry storage conditions(Fig.12.c) .

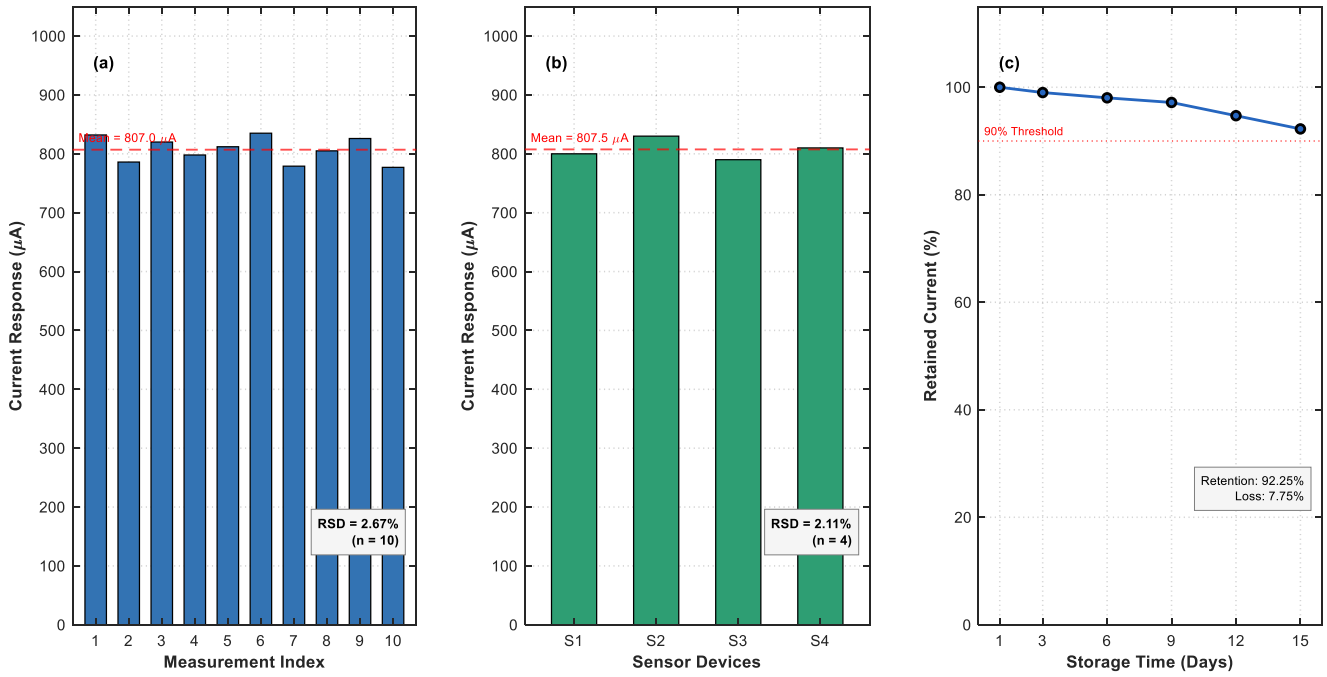


Fig.12.a repeatability (RSD = 2.67%, 10 cycles), 12.b Reproducibility (RSD = 2.11%, n = 4 devices), and 12.c storage stability (92.3% retention over 13 days) of the ESGOT biosensor.

Preliminary correlation with blood glucose

To assess point-of-care utility, clinical feasibility was examined by measuring human saliva samples in parallel with capillary blood glucose readings obtained using a standardized commercial glucometer across 20 healthy volunteers. All human sample collection protocols were conducted in strict accordance with the Declaration of Helsinki, and informed consent was obtained from all participants prior to testing. Salivary glucose levels determined by the side-gate ESGOT correlated positively with blood glucose concentrations across the cohort, yielding a Pearson correlation coefficient of $r = 0.89$ ($R^2 = 0.79$) (Fig.13). These preliminary findings confirm the practical viability of the proposed flexible ESGOT platform for non-invasive metabolic screening. To advance toward robust clinical translation, future work will focus on expanding the clinical cohort, standardizing fasting versus postprandial saliva collection protocols, and integrating multivariate correction algorithms to account for physiological fluctuations in salivary matrix composition.

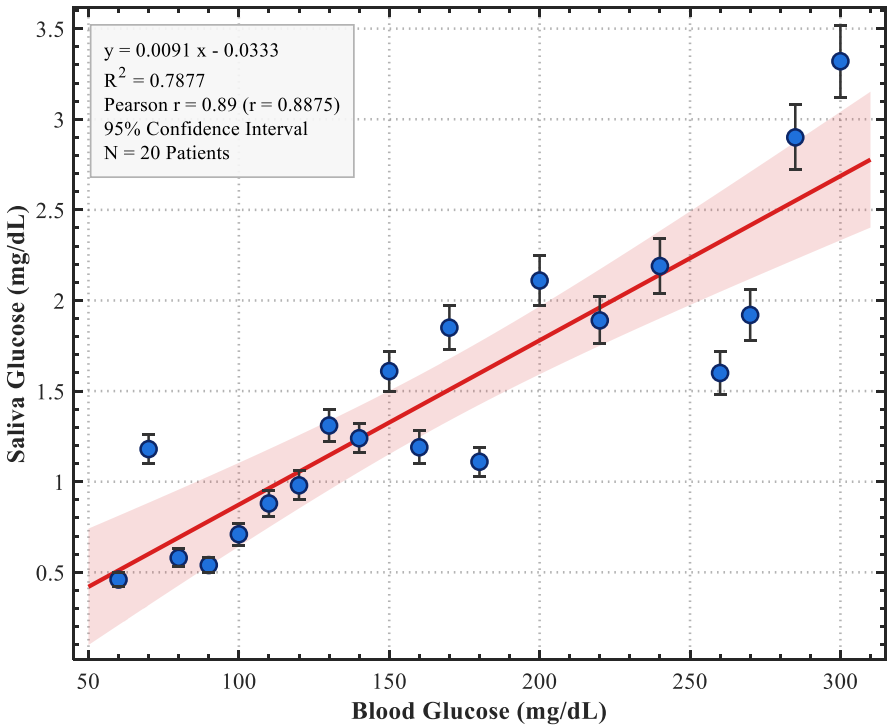


Fig. 13. Correlation between ESGOT-measured salivary glucose and commercial glucometer blood glucose readings (n = 20 volunteers; Pearson r = 0.89, R^2 = 0.79, 95% CI show).

Performance evaluation

To evaluate the performance of the proposed flexible ESGOT biosensor, its key analytical parameters, including the linear dynamic range, limit of detection (LOD), and sensitivity, were compared with recent field-effect and organic transistor-based glucose sensors (TableI). Conventional metal-oxide and nanostructured transistor sensors often require rigid substrates or high-temperature fabrication, while prior organic transistor platforms offer mechanical flexibility but frequently suffer from elevated detection limits (above 20 µM) or limited sub-micromolar resolution in low-concentration regimes such as human saliva [28], [29].

In comparison, the developed flexible ESGOT platform, featuring a solution-processed LiTFSI/tBP-doped Spiro-OMeTAD channel and a coplanar Nafion/GOx-functionalized Cu/Ag side-gate, successfully bridges the gap between high analytical sensitivity and mechanical conformability. Operating within the safe thermodynamic window of water (VDS = −1.0 V and VGS = −0.8 V), the sensor achieves an ultralow limit of detection of 0.81 µM and a dual-regime calibration, including a logarithmic sensitivity of 127.4 µA/decade spanning up to 1000 µM, alongside a high linear sensitivity of 18.21 µA/µM in the low-concentration range. This performance effectively encompasses the physiological salivary glucose window (10–500 µM), confirming that the

coplanar ESGOT architecture provides a highly sensitive, stable, and low-power transducer well-suited for noninvasive wearable point-of-care diagnostics.

Glucose Sensors	Method of Detection	LDR (Linear Range)	LOD	Sensitivity	Ref
Fe_2O_3-ZnO NRs	FET	0.05 - 18 mM	0.012 mM	0.010575 µA/µM	[37]
MoS_2	FET	0.3 µM - 30 mM	0.3 µM	260.75 µA/µM	[19]
In_2O_3	FET	10 nM - 1 mM	0.01 µM	—	[20]
Graphene/Ag	FET	0.1 µM - 0.35 mM	0.0262 µM	9.95961 µA/µM	[27]
Ni/Cu-MOFs	FET	1 µM - 20 mM	0.51 µM	0.026 µA/µM	[17]
P3HT/PVP/Nafion:GOx	OTFT	8 µM - 30 mM	—	Normalized	[29]
Printed OECT (Ag/P3HT/Nafion/GOx)	OECT	0.017 - 0.5 mM	29 µM	—	[28]
Flexible ESGOT (Spiro-OMeTAD/Nafion:GOx)	ESGOT	2.70–10 µM (Linear); 10–1000 µM (Log)	0.81 µM	127.4 (µA/decade) 18.21 µA/µM	This work

TABLE I:Comparison of the analytical performance of the proposed flexible esgot biosensor with recently reported glucose sensors

Conclusion

A flexible, low-voltage coplanar side-gate electrolyte-gated organic transistor (ESGOT) employing a LiTFSI/tBP-doped Spiro-OMeTAD channel and a separate Nafion/GOx-functionalized side-gate electrode on Kapton has been demonstrated for non-invasive salivary glucose sensing. By separating the biorecognition interface at the gate from the organic conduction channel, high enzymatic activity and stable charge transport are achieved simultaneously. Operating at safe

potentials within the electrochemical stability window of water (VDS = -1.0 V, VGS = -0.8 V), the device exhibits a dynamic range of 0.1 to 1000 µM with a logarithmic sensitivity of 127.4 µA/decade, a validated linear quantitative range from the LOQ to 10 µM (2.70 to 10 µM) with a sensitivity of 18.21 µA/µM, a limit of detection (LOD) of 0.81 µM, and a limit of quantification (LOQ) of 2.70 µM. The sensor demonstrated excellent manufacturing consistency (reproducibility RSD = 2.11%), robust operational repeatability (RSD = 2.68%), high selectivity via Donnan exclusion, and 92.3% retention of initial sensitivity after 13 days of storage. These results highlight the promise of flexible coplanar ESGOTs for non-invasive point-of-care diagnostics and continuous wearable metabolic tracking.

Data availability

The datasets used and/or analyzed during the current study available from the corresponding author on reasonable request.

Ethics approval and consent to participate

All procedures involving human participants were conducted in strict accordance with the ethical guidelines of the Declaration of Helsinki and were approved by the **Research Ethics Committee of Shiraz University of Technology** .

The study involved a minimal-risk, non-invasive validation protocol using commercially available finger-prick glucometer reference checks and voluntary saliva donation. Informed written consent was obtained from all 20 healthy adult volunteers prior to sample collection. All individual data were anonymized before analysis.

Authors contributions

M.N., Z.K., and M.H. designed and fabricated the Bio-ESGOFET sensors. All authors reviewed and approved the manuscript.

Funding

The authors received no specific funding for this work.

Competing interests

The authors declare no competing interests.

References

1. Farahmandpour, M., Ansari, H. R. & Kordrostami, Z. Flexible enzyme-free gate engineered bio-FET glucose sensor based on nickel–tungstate microcrystals. IEEE Sensors J. 24, 9308–9316 (2024).

2. Farahmandpour, M., Haghshenas, H. & Kordrostami, Z. Blood glucose sensing by back gated transistor strips sensitized by CuO hollow spheres and rGO. Sci. Rep. 12, 21872 (2022).

3. Farahmandpour, M., Kordrostami, Z., Rajabzadeh, M. & Khalifeh, R. Flexible bio-electronic hybrid metal–oxide channel FET as a glucose sensor. IEEE Trans. Nanobiosci. 22, 855–862 (2023).

4. Wild, S., Roglic, G., Green, A., Sicree, R. & King, H. Global prevalence of diabetes: Estimates for the year 2000 and projections for 2030. Diabetes Care 27, 1047–1053 (2004).

5. Farahmandpour, M., Kordrostami, Z. & Haghshenas, H. Side-Gate-FET test strips for invasive and non-invasive saliva-based glucose monitoring using GO-catalyzed CuO-ZnO hollow spheres. IEEE Sensors J. 25, 30343–30351 (2025).

6. Xu, T. et al. Electrospun CuO-nanoparticles-modified polycaprolactone@polypyrrole fibers: An application to sensing glucose in saliva. Nanomaterials 8, 133 (2018).

7. Coyle, V. E. et al. Co3O4 needles on Au honeycomb as a non-invasive electrochemical biosensor for glucose in saliva. Biosens. Bioelectron. 141, 111479 (2019).

8. Chakraborty, P., Deka, N., Patra, D. C., Debnath, K. & Mondal, S. P. Salivary glucose sensing using highly sensitive and selective nonenzymatic porous NiO nanostructured electrodes. Surf. Interfaces 26, 101324 (2021).

9. Vinita, Nirala, N. R., Tiwari, M. & Prakash, R. A nanoporous palladium(II) bridged coordination polymer acting as a peroxidase mimic in a method for visual detection of glucose in tear and saliva. Microchim. Acta 185, 1–10 (2018).

10. Dehbali, M. M., Farahmandpour, M., Hamedi, S. & Kordrostami, Z. Development of a portable smart glucometer with two-electrode bio-electronic test strip patch based on Cu/Au/rGO/PEDOT:PSS. Sci. Rep. 13, 9505 (2023).

11. Farahmandpour, M., Dideban, D., Dehbali, M. M. & Kordrostami, Z. Disposable wireless FET paper sensor based on MWCNT/MXene/MoS2 composite for non-invasive glucose detection in saliva. J. Alloys Compd. 1014, 178715 (2025).

12. Liu, J., Shi, L., Shi, Y., Zeng, Q. & Yang, Y. Glucose sensing performance of bimetallic MOFs CoFe-ZIF/CC for enzyme-free saliva sensor applications. J. Alloys Compd. 999, 174733 (2024).

13. Wang, M., Wang, H. & Cheng, J. An enzyme-encapsulated metal–organic frameworks nanomesh biosensor for salivary glucose detection. Adv. Mater. Technol. 9, 2301678 (2024).

14. Ahmad, R. et al. Highly efficient non-enzymatic glucose sensor based on CuO modified vertically-grown ZnO nanorods on electrode. Sci. Rep. 7, 5715 (2017).

15. Mishra, A. K., Jarwal, D. K., Mukherjee, B. & Jit, S. CuO nanoparticles decorated ZnO nanorods based extended-gate field-effect-transistor (EGFET) for enzyme-free glucose sensing application. IEEE Trans. Nanobiosci. 21, 3–9 (2022).

16. Naorem, M. & Paily, R. P. Non-enzymatic glucose detection based on GO/Ag nanocomposite in SiO2 trench embedded field effect transistor. IEEE Sensors J. 22, 15614–15621 (2022).

17. Wang, B., Luo, Y., Gao, L., Liu, B. & Duan, G. High-performance field-effect transistor glucose biosensors based on bimetallic Ni/Cu metal-organic frameworks. Biosens. Bioelectron. 171, 112736 (2021).

18. Khan, M. et al. Vertically oriented zinc oxide nanorod-based electrolyte-gated FET for high-performance glucose sensing. Anal. Chem. 94, 8867–8873 (2022).

19. Shan, J. et al. High sensitivity glucose detection at extremely low concentrations using a MoS2-based field-effect transistor. RSC Adv. 8, 7942–7948 (2018).

20. Liu, Q. et al. Highly sensitive and wearable In2O3 nanoribbon transistor biosensors with integrated on-chip gate for glucose monitoring in body fluids. ACS Nano 12, 1170–1178 (2018).

21. Zafar, H., Channa, A., Jeoti, V. & Stojanovic, G. M. Comprehensive review on wearable sweat-glucose sensors for continuous glucose monitoring. Sensors 22, 638 (2022).

22. Wang, B. et al. Wearable aptamer-field-effect transistor sensing system for noninvasive cortisol monitoring. Sci. Adv. 8, eabm0967 (2022).

23. Peng, H.-L., Zhang, Y., Liu, H. & Gao, C. Flexible wearable electrochemical sensors based on AuNR/PEDOT:PSS for simultaneous monitoring of levodopa and uric acid in sweat. ACS Sensors 9, 3296–3306 (2024).

24. Farahmandpour, M. & Kordrostami, Z. Wearable MXene-enhanced organic bio-FET paper patch for glucose detection in sweat with pH and temperature calibration. Sci. Rep. 15, 1–18 (2025).

25. Meng, A. et al. Curly fish scales-like Ni2.5Mo6S6.7 electrodeposited on PEDOT-rGO with uneven surface as ultrafast response electrode for electrocatalytic glucose, nitrite and hydrogen peroxide. J. Colloid Interface Sci. 608, 131–141 (2022).

26. Man, B. et al. MoS2-spaced bimetal composite structure as SERS-SPR sensor for glucose detection. J. Alloys Compd. 902, 163789 (2022).

27. Archana, R. et al. Development of highly sensitive Ag NPs decorated graphene FET sensor for detection of glucose concentration. J. Inorg. Organomet. Polym. Mater. 30, 3818–3825 (2020).

28. Lim, S.-L. et al. Printed organic electronic sensors for glucose detection in human saliva. Appl. Phys. Lett. 127, 243701 (2025).

29. Elkington, D. et al. Detection of saliva-range glucose concentrations using organic thin-film transistors. Appl. Phys. Lett. 105, 043303 (2014).

30. Camarca, A. et al. Emergent biosensing technologies based on fluorescence spectroscopy and surface plasmon resonance. Sensors 21, 906 (2021).

31. Ji, X. et al. Highly sensitive metabolite biosensor based on organic electrochemical transistor integrated with microfluidic channel and Poly(N-vinyl-2-pyrrolidone)-capped platinum nanoparticles. Adv. Mater. Technol. 1, 1600042 (2016).

32. Ait Yazza, A., Blondeau, P. & Andrade, F. J. Simple approach for building high transconductance paper-based organic electrochemical transistor (OECT) for chemical sensing. ACS Appl. Electron. Mater. 3, 1886–1895 (2021).

33. Kousseff, C. J. et al. Single-component electroactive polymer architectures for non-enzymatic glucose sensing. Adv. Sci. 11, 2308281 (2024).

34. Zhou, G., Cao, Z., Liu, Y., Zheng, H. & Xu, K. Highly sensitive and stable glucose sensing using N-type conducting polymer-based organic electrochemical transistor. J. Electroanal. Chem. 952, 117961 (2024).

35. Nguyen-Dang, T. et al. Air-stable perylene diimide trimer material for N-type organic electrochemical transistors. Adv. Mater. 36, 2312254 (2024).

36. Li, Y., Wang, N., Yang, A., Ling, H. & Yan, F. Biomimicking stretchable organic electrochemical transistor. Adv. Electron. Mater. 5, 1900566 (2019).

37. Ahmad, R., Ahn, M.-S. & Hahn, Y.-B. Fabrication of a non-enzymatic glucose sensor field-effect transistor based on vertically-oriented ZnO nanorods modified with Fe2O3. Electrochem. Commun. 77, 107–111 (2017).